Chemical Science

ROYAL SOCIETY OF CHEMISTRY

EDGE ARTICLE

View Article Online
View Journal

Cite this: DOI: 10.1039/d5sc09606e

All publication charges for this article have been paid for by the Royal Society of Chemistry

Oscillator–qubit generalized quantum signal processing: a case study of the uracil cation vibronic model

Jungsoo Hong,[a] Seong Ho Kim,[b] Seung Kyu Min *[b] and Joonsuk Huh *[cd]

Hybrid oscillator–qubit processors have recently demonstrated high-fidelity control of both continuous- and discrete-variable information processing. However, most quantum algorithms remain limited to homogeneous quantum architectures. Here, we present a compiler for hybrid oscillator–qubit processors that implements state preparation and time evolution. In this setting, the compiler invokes generalized quantum signal processing (GQSP) to synthesize arbitrary analytic bosonic phase gates in a constructive manner, with circuit depth scaling as $\mathcal{O}(\log(1/\varepsilon))$. The approximation cost scales with the Fourier bandwidth of the target bosonic phase, rather than with the degree of nonlinearity. Armed with OQ-GQSP, multi-state vibronic coupling Hamiltonian dynamics can be decomposed into state-dependent arbitrary-phase potential propagators, which also enable extension to multi-state systems through the parity-measurement technique. Compared to fully discrete encodings, our approach avoids the overhead of truncating continuous variables, resulting in linear dependence on the number of vibrational modes. We validate our method on the uracil cation, a canonical system whose accurate modeling requires anharmonic vibronic models, and estimate the cost of state preparation and time evolution.

Received 8th December 2025
Accepted 22nd April 2026

DOI: 10.1039/d5sc09606e

rsc.li/chemical-science

1. Introduction

Recent experimental progress in both discrete-variable (DV, qubit) and continuous-variable (CV, oscillator) information processing has established the foundation for hybrid CV–DV quantum architectures.[1] Despite these advancements, applications of hybrid CV–DV processors are still in an early stage of exploration. Conventionally, qubits and oscillators have been employed in complementary roles: qubits provide access to non-Gaussian resources,[2] while oscillators serve as quantum buses mediating entanglement between qubits in quantum platforms such as trapped ions[3] and circuit QED.[4] The hybrid CV–DV architecture exploits both continuous and discrete degrees of freedom and extends their capabilities beyond their auxiliary roles by harnessing native representations of variables and utilizing both types of non-classical operations.

Such hybrid control naturally matches problems where CV and DV degrees of freedom coexist. The simulation of nonadiabatic molecular dynamics, which requires explicit inclusion of electron–nuclear couplings, represents a regime where hybrid oscillator–qubit architectures are expected to outperform homogeneous qubit-based processors and classical methods.[5,6] Simulations of such hybrid CV–DV systems on qubit-only hardware incur additional overheads to represent high-dimensional bosonic operators with binary qubits. Although a single truncated oscillator uses only a logarithmic number of qubits, the dominant overheads lie in arithmetic and phase-synthesis steps. From a classical perspective, multi-configuration time-dependent Hartree (MCTDH)[7] scales exponentially with the number of modes, and linear-vibronic-coupling (LVC) analog quantum simulators[5,8–10] are effectively near-harmonic, failing to capture essential anharmonic effects. This motivates the development of a more general compiler for nonlinear bosonic dynamics on hybrid CV–DV hardware. Recent bosonic quantum device frameworks have extended digital quantum simulation to anharmonic vibrational dynamics.[11,12] Here we focus on the complementary nonadiabatic vibronic dynamics in hybrid oscillator–qubit quantum devices, where anharmonic bosonic phase gates are synthesized conditionally on electronic states within a multistate Hamiltonian.

In this paper, we introduce oscillator–qubit generalized quantum signal processing (OQ-GQSP), a method for synthesizing arbitrary bosonic phase gates. This approach overcomes the challenges of implementing non-Gaussian operations

[a]SKKU Advanced Institute of Nano Technology (SAINT), Sungkyunkwan University, Suwon 16419, Republic of Korea
[b]Department of Chemistry, Ulsan National Institute of Science and Technology, Ulsan 44919, Republic of Korea. E-mail: skmin@unist.ac.kr
[c]Department of Chemistry, Yonsei University, Seoul 03722, Republic of Korea. E-mail: joonsukhuh@yonsei.ac.kr
[d]Department of Quantum Information, Yonsei University, Seoul 03722, Republic of Korea

through a constructive framework that enables robust and analytic determination of gate parameters. OQ-GQSP invokes generalized quantum signal processing (GQSP)[13] in oscillator–qubit architectures, allowing hybrid processors to implement arbitrary analytic potential propagators conditioned on electronic states—an essential capability for simulating nonadiabatic molecular dynamics. We apply this method to the uracil cation,[14] a pyrimidine nucleobase central to understanding RNA radiation damage and photostability, whose ultrafast relaxation through conical intersections (CIs) requires anharmonic models to accurately capture nonadiabatic dynamics.

Because OQ-GQSP inherits the quantum signal processing structure, it supports both coherent[15] and incoherent accumulation schemes for composing multiple OQ-GQSP blocks. In this work, we employ incoherent accumulation, which reduces circuit depth at the cost of heralded measurements. The success probability of heralded measurements increases with circuit depth, enabling a quantitative trade-off analysis for optimizing resource budgets on a given hardware specification.

The hybrid oscillator–qubit quantum architecture organizes the solution into five steps: (i) the application layer defines ultrafast relaxation dynamics as the target problem; (ii) an algorithmic layer realizes this as time evolution under the anharmonic vibronic model; (iii) a compiler layer synthesises the bosonic nonlinear phase gates needed by the anharmonic vibronic model; (iv) the instruction set architecture (ISA) enumerates the native oscillator–qubit operations;[16] (v) finally, the hardware layer comprises trapped ions and circuit-QED that implement those primitives. Each lower layer exists only to support the one above it, guaranteeing that every step of the stack is both necessary for chemical accuracy and sufficiently native for quantum hardware. Fig. 1 provides a visual summary of our workflow, including these layers. We encode the four electronic states of the uracil cation in a qubit-encoding representation, map off-diagonal vibronic couplings to multi-controlled displacement (MCD) gates, and implement diagonal anharmonic potentials through OQ-GQSP. The complete circuit evolves *via* Trotterized time evolution, directly incorporating both linear couplings and nonlinear anharmonic potential effects at each timestep.

The remainder of this paper is organized as follows. The theory section presents the theoretical framework for anharmonic vibronic coupling models and introduces the uracil cation Hamiltonian as our example system. The method section details the compilation stages including the ISA of oscillator–qubit systems and our OQ-GQSP algorithm for implementing anharmonic potentials. The numerical experiments section provides numerical demonstrations of the potential energy surface reconstruction and comparative dynamics simulations. In the resource estimation section, we compare the computing resources and time complexity for simulating the vibronic coupling model. In the discussion and conclusions section, we discuss the challenges of the OQ-GQSP method and compare it with other methods.

2. Theory

2.1. Vibronic coupling Hamiltonian

For a molecule with N electronic states and M mass-frequency scaled normal mode coordinates $\{\hat{Q}_r\}$ ($r \in \{0, \ldots, M-1\}$) with $\hat{P}_r \equiv -i\frac{\partial}{\partial Q_r}$, the vibronic coupling Hamiltonian takes the form:

$$\begin{aligned}\hat{H} &= \mathbb{I}_{\mathrm{el}} \otimes \left(\hat{T} + \hat{V}_0\right) + \hat{W} \\ &= \mathbb{I}_{\mathrm{el}} \otimes \sum_{r=0}^{M-1} \frac{\omega_r}{2}\left(\hat{P}_r^{\,2} + \hat{Q}_r^{\,2}\right) + \sum_{n,m=0}^{N-1} |n\rangle\langle m| \otimes h_{nm}\left(\hat{Q}_0, \ldots, \hat{Q}_{M-1}\right),\end{aligned} \tag{1}$$

where $\hat{T}$ and $\hat{V}_0$ denote the kinetic and potential energy operators, respectively, and $\hat{W}$ describes additional changes in the potential with respect to $\hat{V}_0$. The momentum and position operators can be defined as $\hat{P}_r = i(\hat{a}_r^\dagger - \hat{a}_r)/\sqrt{2}$ and $\hat{Q}_r = (\hat{a}_r^\dagger + \hat{a}_r)/\sqrt{2}$, where $\hat{a}_r$ and $\hat{a}^\dagger$ are the bosonic annihilation and creation operators, respectively with ω_r denoting the harmonic frequency of mode r. The coupling functions $h_{nm}(\{\hat{Q}_r\})$ depend on the position operators and determine both the molecular physics and the computational complexity of the dynamics simulation which can be expanded as $h_{nn}(\{\hat{Q}_r\}) = E_n + \sum_r \kappa_r^{(n)}\hat{Q}_r + \sum_{r,s}\gamma_{rs}^{(n)}\hat{Q}_r\hat{Q}_s + \cdots$ for diagonals and $h_{nm}(\{\hat{Q}_r\}) = \sum_r \lambda_r^{(\mathrm{nm})}\hat{Q}_r + \sum_{r,s}\mu_{rs}^{(\mathrm{nm})}\hat{Q}_r\hat{Q}_s + \cdots$ for off-diagonals ($n \neq m$). Here, reference electronic energies E_n, and coefficients (κ, γ, λ, and μ) can be determined as parameters at the reference geometries. Conventionally, E_n can be included in the reference Hamiltonian $\hat{H}_0$ as $\hat{H}_0 = \mathbb{I}_{\mathrm{el}} \otimes (\hat{T} + \hat{V}_0) + \sum E_n|n\rangle\langle n| \otimes \mathbb{I}_{\mathrm{osc}}$, while $\hat{W}$ is treated as a first-order expansion.[17]

2.2. Hamiltonian of the uracil cation

In this work, we adopt the model Hamiltonian of the uracil cation from ref. 17. The uracil cation is a representative

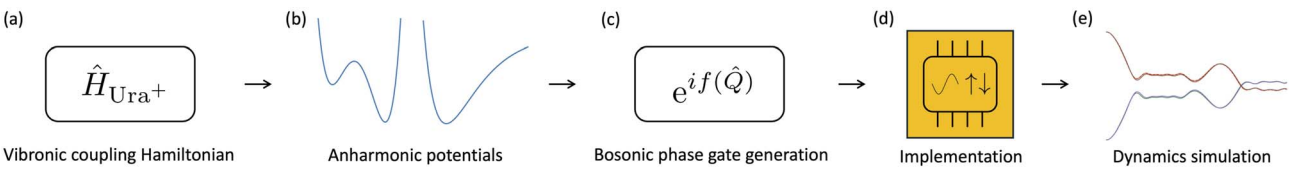

Fig. 1 Quantum simulation workflow for nonadiabatic dynamics of the uracil cation. (a) Target system specified by the vibronic coupling Hamiltonian $\hat{H}_{\mathrm{Ura}^+}$. (b) Anharmonic potential energy surfaces $V(x)$ beyond the harmonic approximation. (c) Construction of nonlinear bosonic phase gates *via* oscillator–qubit generalized quantum signal processing (OQ-GQSP). (d) Implementation on a hybrid oscillator–qubit quantum processor. (e) Measurements yield nonadiabatic electronic population dynamics.

multistate nonadiabatic system with ultrafast relaxation governed by conical intersections after ionization, which has been studied both experimentally and theoretically.[14,17–20] The model includes the four ionic states $\{|D_0\rangle, \ldots, |D_3\rangle\}$, which correspond to $D_0(A'')$, $D_1(A')$, $D_2(A'')$, and $D_3(A')$ at the planar C_s reference geometry. Based on the photoelectron (PE) spectra, the symmetry of electronic states and normal modes, and the adopted reduced parametrization of the reference model, the resulting Hamiltonian can be written as

$$\hat{H}_{\mathrm{Ura}^+} = \hat{H}_0 + \sum_{n=0}^{N-1} |n\rangle\langle n| \otimes \sum_{r=0}^{M-1} f_r^{(n)}\left(\hat{Q}_r\right) + \sum_{\substack{n,m=0 \\ n\neq m}}^{N-1} |n\rangle\langle m| \otimes \sum_{r=0}^{M-1} \lambda_r^{(nm)} \hat{Q}_r, \quad (2)$$

with selected vibrational modes of a' and a'' symmetry from the reference geometry, where $f_r^{(n)}(\hat{Q}_r)$ is a single-mode function neglecting diagonal mode–mode couplings. Under planar C_s symmetry, first-order interstate couplings between states of different symmetry are mediated by a'' modes. In the adopted reduced parametrization of ref. 17, bilinear diagonal intermode terms $\gamma_{rs}^{(n)}(r \neq s)$ and all second- (or higher-) order interstate terms $\mu_{rs}^{(nm)}$ were omitted because their fitted magnitudes were negligible for reproducing the PE spectra, while diagonal second-order terms were retained only in the single-mode form $\gamma_{rr}^{(n)}$. A proper treatment of the neglected multidimensional terms would also require a substantial increase in the fitting effort.

Once one adopts $f_r^{(n)}(\hat{Q}_r) = \kappa_r^{(n)}\hat{Q}_r + \gamma_r^{(n)}\hat{Q}_r^2$, the Hamiltonian reduces to the quadratic vibronic coupling (QVC) model. However, the limitations of the QVC approximation are numerically demonstrated in SI II. To accurately reproduce the PE spectra, higher-order anharmonic terms such as $k_r^{(n)}\hat{Q}_r^4$ and Morse potentials $V_r^{(n)}(\hat{Q}_r)$ are introduced, replacing the harmonic potential $\frac{\omega_r}{2}\hat{Q}_r^2$ in $\hat{H}_0$. Fig. 2 shows the form of the model Hamiltonian without $\hat{H}_0$, coupled to the important normal mode coordinates. For the uracil cation, Morse functions for bond-stretching modes (ν_{24}, ν_{25}, and ν_{26}) and quartic functions for out-of-plane deformations (ν_{10} and ν_{12}) are introduced. The off-diagonal elements between $|D_0\rangle$ and $|D_3\rangle$ or between $|D_2\rangle$ and $|D_3\rangle$ are non-zero in principle because they are symmetry-allowed through a'' modes, but in the adopted reduced model they were treated as negligible and therefore set to zero. The specific parameter values are tabulated in ref. 17 and 21 and also given in Tables S.1–S.3 of SI I.

3. Method

We now present our method for simulating the uracil cation Hamiltonian on oscillator–qubit quantum processors. Our approach exploits the natural correspondence between molecular degrees of freedom and quantum hardware where the electronic states map to qubits while vibrational modes map to quantum oscillators. The key challenge lies in implementing the anharmonic diagonal potentials that go beyond the native instruction set of current hybrid oscillator–qubit quantum platforms.

Modern trapped-ion and circuit QED platforms provide an ISA that includes conditional displacements, conditional phase space rotations, and multi-qubit gates.[1,16] Our compilation strategy systematically translates the molecular Hamiltonian into sequences of these hardware-native operations. The compilation proceeds in three stages: (1) encoding electronic states using an inverted unary representation that facilitates multi-level control operations, (2) implementing off-diagonal linear couplings through MCD gates, and (3) realizing diagonal anharmonic potentials *via* OQ-GQSP that extends the capabilities of the basic instruction set.

3.1. Electronic state encoding

For the N-level electronic system, we employ inverted unary encoding using N qubits, where each computational basis state has exactly one qubit in the $|0\rangle$ state. For the uracil cation's four electronic states, the mapping is:

$$|D_0\rangle \mapsto |1110\rangle, |D_1\rangle \mapsto |1101\rangle, |D_2\rangle \mapsto |1011\rangle, |D_3\rangle \mapsto |0111\rangle. \quad (3)$$

This encoding offers two critical advantages over binary representations. First, it enables direct implementation of electronic transitions $|D_n\rangle\langle D_n|$ using two-body operations on qubits n and m, minimizing the additional complex multi-qubit gates required in binary encoding. Second, the redundancy of unary basis states reduces unwanted interference when applying OQ-GQSP to different electronic subspaces—a crucial requirement for implementing block-diagonal anharmonic potentials. The choice of inverted unary encoding over ordinary unary encoding is motivated by its natural alignment with the

$$\begin{pmatrix}
\sum_{r\in\{3,7,11,18-21\}} \kappa_r^{(0)}\hat{Q}_r + \sum_{r\in\{3,18-21\}} \gamma_r^{(0)}\hat{Q}_r^2 + \sum_{r\in\{10,12\}} k_r^{(0)}\hat{Q}_r^4 + \sum_{r\in\{24-26\}} V_r^{(0)}(\hat{Q}_r) & \sum_{r\in\{10,12\}} \lambda_r^{(01)}\hat{Q}_r & \sum_{r\in\{7,11,18-20,25,26\}} \lambda_r^{(02)}\hat{Q}_r & 0 \\
\sum_{r\in\{10,12\}} \lambda_r^{(01)}\hat{Q}_r & \sum_{r\in\{3,7,11,18-21\}} \kappa_r^{(1)}\hat{Q}_r + \sum_{r\in\{3,18-21\}} \gamma_r^{(1)}\hat{Q}_r^2 + \sum_{r\in\{10,12\}} k_r^{(1)}\hat{Q}_r^4 + \sum_{r\in\{24-26\}} V_r^{(1)}(\hat{Q}_r) & \sum_{r\in\{10,12\}} \lambda_r^{(12)}\hat{Q}_r & \sum_{r\in\{11,18,19,21,24,25,26\}} \lambda_r^{(13)}\hat{Q}_r \\
\sum_{r\in\{7,11,18-20,25,26\}} \lambda_r^{(02)}\hat{Q}_r & \sum_{r\in\{10,12\}} \lambda_r^{(12)}\hat{Q}_r & \sum_{r\in\{3,7,11,18-21\}} \kappa_r^{(2)}\hat{Q}_r + \sum_{r\in\{3,18-21\}} \gamma_r^{(2)}\hat{Q}_r^2 + \sum_{r\in\{10,12\}} k_r^{(2)}\hat{Q}_r^4 + \sum_{r\in\{24-26\}} V_r^{(2)}(\hat{Q}_r) & 0 \\
0 & \sum_{r\in\{11,18,19,21,24,25,26\}} \lambda_r^{(13)}\hat{Q}_r & 0 & \sum_{r\in\{3,7,11,18-21\}} \kappa_r^{(3)}\hat{Q}_r + \sum_{r\in\{3,18-21\}} \gamma_r^{(3)}\hat{Q}_r^2 + \sum_{r\in\{24-26\}} V_r^{(3)}(\hat{Q}_r)
\end{pmatrix}$$

Fig. 2 Four-state vibronic coupling model Hamiltonian for the uracil cation. $V_r^{(\alpha)}(\hat{Q}_r) = d_r^{(\alpha)}\left[e^{(a_r^{(\alpha)})(\hat{Q}_r - q_{r,0}^{(\alpha)})} - 1\right]^2 + e_r^{(\alpha)}$ is the Morse potential.

original GQSP signal operator. Ordinary unary encoding is also compatible with our construction and the two choices differ only by single-qubit Pauli X gates in computational cost.

3.2. Compilation of off-diagonal couplings

The off-diagonal terms in the vibronic Hamiltonian encode the coupling between electronic states induced by the nuclear motion, driving nonadiabatic dynamics through CIs. These LVCs $|D_n\rangle\langle D_m|\otimes\hat{Q}_r$ translate naturally to MCD operations in oscillator–qubit architectures.[22]

The ISA of oscillator–qubit platforms provides the building blocks for constructing MCD gates.[1] The conditional displacement (CD) gate $\mathrm{CD}_{q,r}(\theta)$: $= |0\rangle_q\langle 0|_q\otimes e^{+i\theta\hat{Q}_r} + |1\rangle_q\langle 1|_q\otimes e^{-i\theta\hat{Q}_r}$ implements spin-dependent position displacements and serves as the primary gate throughout the compilation stages. In trapped ions, this is realized through red and blue sideband transitions that produce state-dependent forces.[23] Circuit QED achieves the same operation through echoed conditional displacement (ECD) sequences with dispersive coupling between transmon qubits and microwave cavities.[4] Additionally, two-qubit gates and single qubit Clifford gates complete our native instruction set for constructing MCD operations. For example, the vibronic interaction between $|D_0\rangle$ and $|D_1\rangle$ can be decomposed as:

$$\begin{aligned} e^{i\hat{H}_{\mathrm{off}}^{(01)}\Delta t}|\psi\rangle &= e^{i\theta(|D_0\rangle\langle D_1|+|D_1\rangle\langle D_0|)\hat{Q}}|\psi\rangle \\ &= e^{i\theta(|1110\rangle\langle 1101|+|1101\rangle\langle 1110|)\hat{Q}}|\psi\rangle \\ &= e^{i\theta\left(\widehat{\sigma_x^{(1)}\sigma_x^{(0)}}+\widehat{\sigma_y^{(1)}\sigma_y^{(0)}}\right)\hat{Q}|\psi\rangle} \\ &= e^{i\theta\widehat{\sigma_x^{(1)}\sigma_x^{(0)}}\hat{Q}e^{i\theta\widehat{\sigma_y^{(1)}\sigma_y^{(0)}}\hat{Q}|\psi\rangle}}, \end{aligned} \tag{4}$$

where $|\psi\rangle$ is the state in the inverted unary encoded space and $\hat{\sigma_k^{(i)}}$, ($k\in\{x,y,z\}$ and $i\in\{0,1,2,3\}$) is a Pauli operator acting on the i th qubit. The inverted unary encoding simplifies these implementations: the MCD gate for transition $n\leftrightarrow m$ requires only controlled operations on qubits n and m, resulting in constant gate depth independent of the number of electronic states.

This set of operations is capable of directly implementing nonadiabatic dynamics of multilevel linear couplings and harmonic potentials, while this instruction set still cannot implement anharmonic terms that are essential for accurate molecular dynamics.

3.3. Compilation of anharmonic diagonal potentials

The primary challenge in simulating the nonadiabatic dynamics of the uracil cation on an oscillator–qubit processor lies in implementing physics-inspired potentials, such as the Morse potential. While polynomial potentials can, in principle, be constructed *via* conventional methods using Baker–Campbell–Hausdorff (BCH) expansions, the overhead and inefficiency of synthesizing each term motivate us to explore alternative approaches. Moreover, the diversity of physically motivated functional forms necessitates a fundamentally different compilation strategy—one that can systematically and uniformly represent arbitrary potentials. To this end, we aim to construct a nonlinear bosonic phase gate that approximates arbitrary functions within a reliable error bound and remains robust under arbitrary quantum states, thereby enabling its direct use as a gate in quantum simulations.

The key insight is that a sequence of non-commuting gates can effectively accumulate nonlinear effects.[24] Rather than explicitly reconstructing interaction terms order by order and canceling unwanted contributions *via* BCH expansions, Park *et al.*[25] employed a direct Fourier series approximation with iterative non-commuting Rabi gates. Using this method, for example, a quartic potential term such as $\exp(i0.2\hat{Q}^4)$ can be approximated with ten Rabi gates, achieving a fidelity of 0.9932.

A critical caveat in applying such gates to quantum dynamics is the vacuum-state dependence of the synthesized nonlinear bosonic phase gates. This dependence can introduce systematic errors when acting on general time-evolved states beyond the initial vacuum state. Notably, the iterative structure of Rabi gate sequences[25] for generating Fourier series functions is formally analogous to quantum signal processing (QSP) applied to the oscillator–qubit hybrid system. QSP can represent a continuous function of the matrix with non-commuting sequences where angle parameters can be efficiently calculated.[26,27] As typically used with QSP, Jacobi–Anger expansions with Chebyshev polynomials may offer improved robustness and convergence than Fourier series approximations. However, their implementation requires direct block encodings of bosonic operators such as $\begin{bmatrix}\hat{Q} & *\\ * & *\end{bmatrix}$—which, to the best of our knowledge, remains infeasible on hybrid oscillator–qubit architectures. In particular, ref. 28 demonstrates a QSP implementation on hybrid architectures by block-encoding bosonic phase operators using the CD gate, which acts as a Z-basis signal operator.

Within the conventional QSP framework, one aims to represent $e^{-ix\tau}$ approximately by a polynomial in the input variable x, later promoted to the operator or Hamiltonian, with τ denoting a real parameter corresponding to the effective simulation time.[29] However, as emphasized in ref. 29, this approach encounters fundamental limitations. The standard QSP constructs real polynomials with fixed parity in default. Extending the class of functions that can be approximated beyond even or odd requires additional circuit depth of linear combination of unitaries.

GQSP[13] lifts these limitations by generalizing the signal operator from $U(1)$ rotations to SU(2) rotations, and by introducing an asymmetric signal operator of the form $\hat{A}_{\hat{U}} = \begin{bmatrix}\hat{U} & 0\\ 0 & I\end{bmatrix}$. This generalization eliminates the parity constraints and permits the construction of polynomials with arbitrary complex coefficients. The theorem of GQSP is often stated as follows for the case including positive and negative powers of a Laurent polynomial:[13,26,30]

Theorem 1 (Generalized Quantum Signal Processing (GQSP)[13]). Let $\phi = (\phi_{-d}, \ldots, \phi_d)$ and $\theta = (\theta_{-d}, \ldots, \theta_d)$. For any $d\in\mathbb{N}$, there exist parameters $\theta, \phi\in\mathbb{R}^{2d+1}$ and $\lambda\in\mathbb{R}$ such that:

$$\mathrm{e}^{\mathrm{i}\lambda\widehat{\sigma}_z}\mathrm{e}^{\mathrm{i}\phi_{-d}\widehat{\sigma}_x}\mathrm{e}^{\mathrm{i}\theta_{-d}\widehat{\sigma}_z}\left(\prod_{r=-d+1}^{0}\hat{B}\mathrm{e}^{\mathrm{i}\phi_r\widehat{\sigma}_x}\mathrm{e}^{\mathrm{i}\theta_r\widehat{\sigma}_z}\right)\left(\prod_{r=1}^{d}\hat{A}\mathrm{e}^{\mathrm{i}\phi_r\widehat{\sigma}_x}\mathrm{e}^{\mathrm{i}\theta_r\widehat{\sigma}_z}\right) = \begin{bmatrix} F(x) & -(G(x))^* \\ G(x) & (F(x))^* \end{bmatrix}, \tag{5}$$

for all $x\in\mathbb{T}$, where $\mathbb{T}=\{x\in\mathbb{C}:|x|=1\}$ and

$$\begin{aligned}\hat{A} &= \left(|0\rangle_q\langle 0|_q\otimes x\right)+\left(|1\rangle_q\langle 1|_q\otimes\mathbb{I}\right) = \begin{bmatrix} x & 0\\ 0 & 1\end{bmatrix},\\ \hat{B} &= \left(|0\rangle_q\langle 0|_q\otimes\mathbb{I}\right)+\left(|1\rangle_q\langle 1|_q\otimes x^{-1}\right) = \begin{bmatrix} 1 & 0\\ 0 & x^{-1}\end{bmatrix},\end{aligned} \tag{6}$$

if and only if:

1. $F, G\in\mathbb{C}[x]$ with $|\deg(f)|,\ |\deg(G)|\le d$.
2. $|F(\mathrm{x})|^2+|G(x)|^2=1$

In ref. 13, generating nonlinear phase functions *via* GQSP proceeds through a two-step approximation strategy. First, the target potential $V(\mathrm{x})$ is approximated by a truncated Fourier series. Second, each exponential term of the form $\exp(\mathrm{i}a_n\cos(nx))$ or $\exp(\mathrm{i}b_n\sin(nx))$ is further expanded using the Jacobi–Anger identity:

$$\begin{aligned}\exp\left(\mathrm{i}V\left(\hat{Q}\right)\Delta t\right) &\approx \exp\left(\mathrm{i}\Delta t\sum_n\left[a_n\cos\left(\frac{\pi}{L}n\hat{Q}\right)+b_n\sin\left(\frac{\pi}{L}n\hat{Q}\right)\right]\right)\\ &\approx \prod_k\left(\sum_n i^n J_n(a_k\Delta t)\mathrm{e}^{\mathrm{i}\frac{\pi}{L}nk\hat{Q}}\right)\left(\sum_n J_n(b_k\Delta t)\mathrm{e}^{\mathrm{i}\frac{\pi}{L}nk\hat{Q}}\right),\end{aligned} \tag{7}$$

where the Jacobi–Anger expansions are

$$\mathrm{e}^{\mathrm{i}t\cos\theta}=\sum_{n=-\infty}^{\infty}i^nJ_n(t)\mathrm{e}^{\mathrm{i}n\theta},\quad \mathrm{e}^{\mathrm{i}t\sin\theta}=\sum_{n=-\infty}^{\infty}J_n(t)\mathrm{e}^{\mathrm{i}n\theta}, \tag{8}$$

and J_n denotes the n-th Bessel function of the first kind. This indirect construction incurs additional overhead due to the nested use of both Fourier and Jacobi–Anger expansions.

As an alternative, we adopt a direct Fourier-based approach in which the nonlinear bosonic phase gate $\exp(\mathrm{i}V(\hat{Q})\Delta t)$ is expressed as a Laurent polynomial:

$$\exp\left(\mathrm{i}V\left(\hat{Q}\right)\Delta t\right)\approx\sum_{n=-d}^{d}c_n\left(\mathrm{e}^{\mathrm{i}\frac{\pi}{L}\hat{Q}}\right)^n, \tag{9}$$

where $c_n\in\mathbb{C}$ are Fourier coefficients and V is an analytic potential function. This formulation is natively compatible with GQSP and avoids the compounded approximation cost associated with the Jacobi–Anger expansion.

We now apply GQSP (Theorem 1) to oscillator–qubit processors. The first step is to construct the GQSP signal operators from native bosonic gates. On both trapped-ion[31] and circuit-QED[4,32] platforms, the Z-basis controlled displacement $\mathrm{CD}_z(\xi)=\mathrm{e}^{\mathrm{i}\xi\hat{\sigma}_z\hat{Q}}$ and the unconditional displacement $D(\xi)=\mathrm{e}^{\mathrm{i}\xi\hat{Q}}$ are native operations. With $\hat{U}=\mathrm{e}^{\mathrm{i}\pi\hat{Q}/L}$, the complementary signal operators

$$A_{\hat{Q}}=\begin{bmatrix}\hat{U} & 0\\ 0 & \mathbb{I}_{\mathrm{osc}}\end{bmatrix},\quad B_{\hat{Q}}=\begin{bmatrix}\mathbb{I}_{\mathrm{osc}} & 0\\ 0 & \hat{U}^\dagger\end{bmatrix} \tag{10}$$

are constructed without *ancilla qubits* using $A_{\hat{Q}}=\mathrm{CD}_z(\pi/2L)\cdot D(\pi/2L)$: the $|0\rangle_q$ component acquires displacement $\mathrm{e}^{\mathrm{i}(+\pi/2L+\pi/2L)\hat{Q}}=\hat{U}$, while the $|1\rangle_q$ component sees $\mathrm{e}^{\mathrm{i}(-\pi/2L+\pi/2L)\hat{Q}}=\mathbb{I}_{\mathrm{osc}}$, and $B_{\hat{Q}}$ follows analogously. Inserting these into the GQSP circuit of Theorem 1 yields the OQ-GQSP operator (Fig. 3):

$$\mathrm{OQ-GQSP}:=\mathrm{e}^{\mathrm{i}\lambda\widehat{\sigma}_z}\mathrm{e}^{\mathrm{i}\phi_{-d}\widehat{\sigma}_x}\mathrm{e}^{\mathrm{i}\theta_{-d}\widehat{\sigma}_z}\left(\prod_{r=-d+1}^{0}\hat{B}_{\hat{Q}}\mathrm{e}^{\mathrm{i}\phi_r\widehat{\sigma}_x}\mathrm{e}^{\mathrm{i}\theta_r\widehat{\sigma}_z}\right)\left(\prod_{r=1}^{d}\hat{A}_{\hat{Q}}\mathrm{e}^{\mathrm{i}\phi_r\widehat{\sigma}_x}\mathrm{e}^{\mathrm{i}\theta_r\widehat{\sigma}_z}\right)=\begin{pmatrix}F\left(\hat{U}\right) & -\left(G\left(\hat{U}\right)\right)^\dagger\\ G\left(\hat{U}\right) & \left(F\left(\hat{U}\right)\right)^\dagger\end{pmatrix}, \tag{11}$$

where $F(\hat{U})=\sum_{n=-d}^{d}c_n\mathrm{e}^{\mathrm{i}n\pi\hat{Q}/L}$ is an arbitrary degree-d Fourier series of the bosonic phase operator with period $2L$. Unlike the previous hybrid oscillator–qubit Z-basis QSP,[28] OQ-GQSP removes parity restrictions on the Fourier series, enabling the synthesis of arbitrary bosonic phase functions. Given a target $F(\hat{U})$ satisfying the GQSP admissibility conditions of Theorem 1, the required angle parameters $\theta,\phi\in\mathbb{R}^{2d+1}$ and $\lambda\in\mathbb{R}$ are obtained by classical preprocessing: the inverse nonlinear Fast Fourier Transform on SU(2),[27] which recovers all $4d+3$ angles in $\mathcal{O}(d\log^2 d)$ time with numerical stability. Armed with this construction, state-dependent nonlinear bosonic phase gates can be implemented on a hybrid oscillator–qubit processor as depicted in Fig. 4.

Lemma 1 (OQ-GQSP for a state-dependent nonlinear bosonic phase gate). Given a state in oscillator–qubit processor $|\psi_D\rangle|\mathrm{osc}\rangle|0\rangle_a$ with inverted-unary-encoded qubits $|\psi_D\rangle=a_0|D_0\rangle+a_1|D_1\rangle+a_2|D_2\rangle+a_3|D_3\rangle$, an oscillator $|\mathrm{osc}\rangle$, and an ancilla qubit $|0\rangle_a$, we can implement a state-dependent nonlinear bosonic phase gate $\mathrm{e}^{\mathrm{i}|D_n\rangle\langle D_n|V_{nr}(\hat{Q}_r)}$ with two OQ-GQSP operators and two measurements, each with success probability $1-\delta$ where $\delta=\|G(\hat{U})\|2\ll 1$.

This lemma completes our ISA for simulating anharmonic vibronic dynamics. The inverted unary encoding enables selective application of anharmonic potentials. The high success probability $(1-\delta)$ with $\delta\ll 1$ makes this approach feasible for dynamical simulations of intermediate-sized molecules. Fig. 4 depicts the circuit implementation, showing how the ancilla qubit mediates between the electronic state and the oscillator to produce the desired state-dependent evolution.

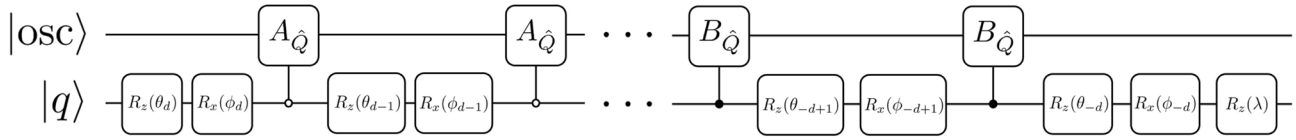

Fig. 3 Quantum circuit for OQ-GQSP. $|\mathrm{osc}\rangle$ is a quantum oscillator and $|q\rangle$ is a qubit register. The left half of the circuit generates positive powers, and the right half generates negative powers of the Laurent (Fourier) series terms.

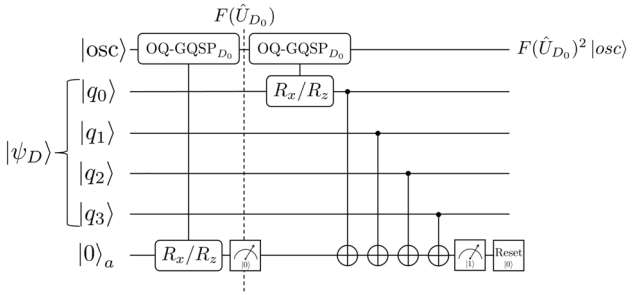

Fig. 4 Quantum circuit for a state-dependent nonlinear bosonic phase gate with OQ-GQSP. $|\psi_D\rangle$ is an electronic state encoded with unary code.

With both off-diagonal linear couplings *via* MCD gates and diagonal anharmonic potentials *via* OQ-GQSP now compilable, we can construct the complete quantum circuit for simulating uracil cation dynamics. Moreover, when the off-diagonal coupling itself is anharmonic, *i.e.* $(|n\rangle\langle m| + |m\rangle\langle n|)\otimes f_{nm,r}(\hat{Q}_r)$ with a nonlinear $f_{nm,r}$, the corresponding propagator can be reduced to two diagonal state-dependent OQ-GQSP blocks by diagonalizing the electronic transition operator *via* a two-level Givens rotation on the $\{|n\rangle, |m\rangle\}$ subspace (SI III D).

3.4. Trotterization and circuit structure

Based on the OQ-GQSP construction and Lemma 1, we now describe the complete circuit for simulating the vibronic coupling Hamiltonian (2). Let N be the number of electronic states, M the number of vibrational modes, and fix the spectral domain of the position operator $[-L, L]$. For each pair (n, r), define $g_{nr}(x) := \exp(\mathrm{i}\Delta t f_{nr}(x))$, assumed to satisfy the analyticity hypotheses stated in SI III. The first-order Trotter decomposition of a single time step Δt reads

$$\mathrm{e}^{-\mathrm{i}\hat{H}_{\mathrm{VC}}\Delta t} \approx \left(\prod_{r=0}^{M-1}\prod_{n=0}^{N-1} \mathrm{e}^{-\mathrm{i}\hat{H}_{\mathrm{diag}}^{(n,r)}\Delta t}\right)\left(\prod_{r=0}^{M-1}\prod_{\substack{n,m=0\\ n\neq m}}^{N-1} \mathrm{e}^{-\mathrm{i}\hat{H}_{\mathrm{off}}^{(n,m,r)}\Delta t}\right) + \mathcal{O}(\Delta t^2), \tag{12}$$

where $\hat{H}_{\mathrm{diag}}^{(n,r)}$ contains both harmonic and anharmonic contributions for electronic state n and mode r, while $\hat{H}_{\mathrm{off}}^{(n,m,r)}$ represents the LVC between states n and m through mode r. Diagonal terms are implemented with OQ-GQSP or standard CD gates for harmonic potentials, and off-diagonal terms with MCD gates.

To simulate the electronic population dynamics $P_n(t) = \langle\psi(t)|\hat{P}_n|\psi(t)\rangle$ with $\hat{P}_n = |D_n\rangle\langle D_n|\otimes\mathbb{I}_{\mathrm{osc}}$, we evolve the initial state $|\psi_0\rangle$ for total time t divided into p Trotter steps (Fig. 5). We target a total simulation error ε split equally between Trotterization and Fourier truncation: $\varepsilon_{\mathrm{Trot}} = \varepsilon_{\mathrm{Fourier}} = \varepsilon/2$. Using the standard first-order product-formula error bound[33] $\|U(t) - U_{\mathrm{Trot}}(t;p)\| \leq \Gamma t^2/p$, where Γ is a commutator bound, the number of Trotter steps is $p = \lceil \Gamma t^2/\varepsilon_{\mathrm{Trot}}\rceil$ with $\Delta t = t/p$.

3.5. Fourier truncation and gate count

OQ-GQSP approximates each diagonal propagator $g_{nr}(x) = \exp(\mathrm{i}\Delta t f_{nr}(x))$ using a degree-d Fourier series:

$$g_{nr}(x) = \sum_{k=-d}^{d} c_k^{(nr)} \mathrm{e}^{\mathrm{i}\frac{\pi k}{L}x} + R_{nr}^{(d)}(x), \quad \|R_{nr}^{(d)}\|_\infty \leq \varepsilon_{\mathrm{Fourier}}. \tag{13}$$

By the strip-analytic Fourier-extension bound (Lemma 2 in SI III), the required degree is $d = \mathcal{O}(\ln MN/\varepsilon_{\mathrm{fourier}})$. Lemma 1 then implements each state-dependent propagator $\mathrm{e}^{-\mathrm{i}\hat{H}_{\mathrm{diag}}^{(n,r)}\Delta t} = |n\rangle\langle n|\otimes g_{nr}(\hat{Q}_r)$ with $\mathcal{O}(d)$ CD gate queries.

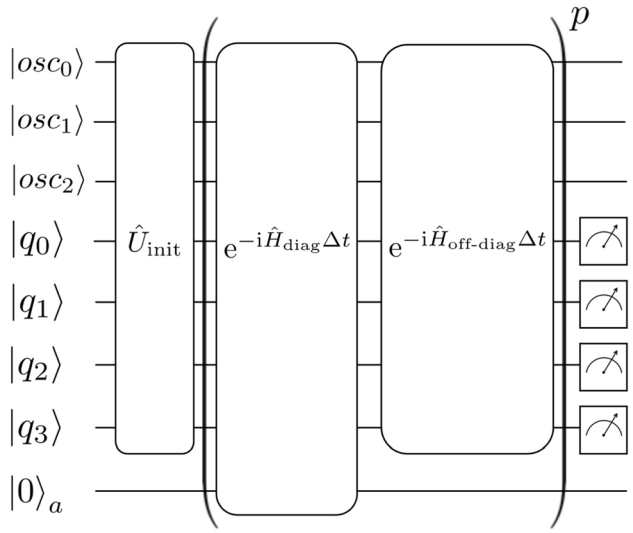

Fig. 5 Abstract quantum circuit for uracil cation Hamiltonian dynamics simulation with $N = 4$ electronic states and $M = 3$ vibrational modes. The circuit consists of three stages: (i) initialization in a product state, (ii) Trotterized time evolution alternating between off-diagonal couplings and diagonal potentials, and (iii) measurement of electronic populations.

3.6. Success probability

Since g_{nr} is a pure phase ($|g_{nr}| = 1$), the GQSP unitarity constraint $|F|^2 + |G|^2 = 1$ (Theorem 1) together with the Fourier-extension truncation bound $\|F - g_{nr}\| \leq \varepsilon_{\text{trunc}}$ (Lemma 2 in SI III) yields $\delta = \|G\|^2 = \mathcal{O}(\varepsilon_{\text{trunc}}) = \mathcal{O}(\rho_{\text{FE}}^{-d}) = \mathcal{O}(e^{-\alpha d})$, where $\varepsilon_{\text{trunc}}$ is the Fourier-extension truncation error, $\rho_{\text{FE}} = e^{\pi\sigma/L_{\text{eff}}} > 1$ is the geometric convergence rate, $L_{\text{eff}} = \tau L$ is the enlarged Fourier-extension period with $\tau > 1$, and σ is the strip half-width of the holomorphic extension; see SI III C for the full derivation. The GQSP phase factors, computed *via* the inverse nonlinear FFT on SU(2),[27] amplify errors by at most poly(d) $\ll e^{\alpha d}$, preserving the exponential convergence. Choosing $d = \mathcal{O}(\ln(\text{MN}/\varepsilon_{\text{Fourier}}))$ yields $\delta = \mathcal{O}(\varepsilon_{\text{Fourier}}/(MN))$, so that $(1-\delta)^{2MN} = \mathcal{O}(1)$, with the success-probability overhead absorbed into a constant factor.

3.7. Total cost

Per Trotter layer, the NM diagonal blocks contribute $\mathcal{O}(NM \ln(MN/\varepsilon_{\text{Fourier}}))$ CD queries, and the off-diagonal LVC terms (already linear, requiring no Fourier expansion) contribute $\mathcal{O}(N^2M)$ MCD queries. The total gate count per Trotter step is therefore

$$\mathcal{O}\big(NM \ln(MN/\varepsilon) + N^2M\big). \tag{14}$$

4. Numerical experiments

We present numerical experiments for OQ-GQSP and its application to state preparation and nonadiabatic dynamics. These experimental results support the OQ-GQSP construction and Lemma 1 by numerically verifying the predicted scaling and accuracy of OQ-GQSP.

4.1. State preparation with nonlinear bosonic phase gates

We first examine the construction of a state-dependent Morse potential for the ν_{26} carbonyl stretch mode in the D_2 electronic state. This mode exhibits strong anharmonicity in the uracil cation system.

Fig. 6 presents the Wigner function representation of the target and approximated gates. The target gate implements the Morse potential $V_{26}^{(D_2)}(\hat{Q})$ for a time step $\Delta t = 3.0$ fs. Using $d = 39$ Fourier components, the initial OQ-GQSP approximation achieves a fidelity of $F = |\langle\psi_0|\hat{U}_{\text{target}}^{\dagger}\hat{U}_{\text{OQ-GQSP}}|\psi_0\rangle|^2 = 0.9229$ for the general state. The truncation error ε can be reduced by increasing the number of Fourier series terms $d = \mathcal{O}(\ln(\varepsilon^{-1}))$, and the proof is given in SI III. The characteristic interference pattern visible in Fig. 6(b) stems from the finite Fock state truncation with the iterative gate sequence from OQ-GQSP.

To improve the approximation, we employ a local optimization procedure that refines the GQSP angles $\{\theta_j, \phi_j, \lambda\}$ to maximize the fidelity with vacuum-state dependency. This approach works well for dynamics near the reference geometry or initial state preparation prior to bosonic algorithms such as analog quantum phase estimation.[34] However, general applications with significant vibrational excitation may require the unoptimized gates to maintain robust accuracy across the full phase space. After optimization, the fidelity improves to 0.9999, with the Wigner function becoming visually indistinguishable from the target (Fig. 6(c)).

4.2. Nonadiabatic dynamics simulation

To validate the OQ-GQSP method for molecular dynamics, we numerically simulate the time evolution of a reduced 2-mode model of the uracil cation including the significant modes in energy spectra ν_{21} and the anharmonic mode ν_{26} represented by a Morse potential.

We initialize the system in electronic states D_3 and D_2 with the anharmonic mode ν_{26} in its vibrational ground state. The dominant spectral mode ν_{21} is displaced by -4 atomic units from its ground state, corresponding to vertical excitation from the neutral molecule. Fig. 7 shows the electronic population dynamics over 80.1 fs for the three levels of approximation defined in the caption.

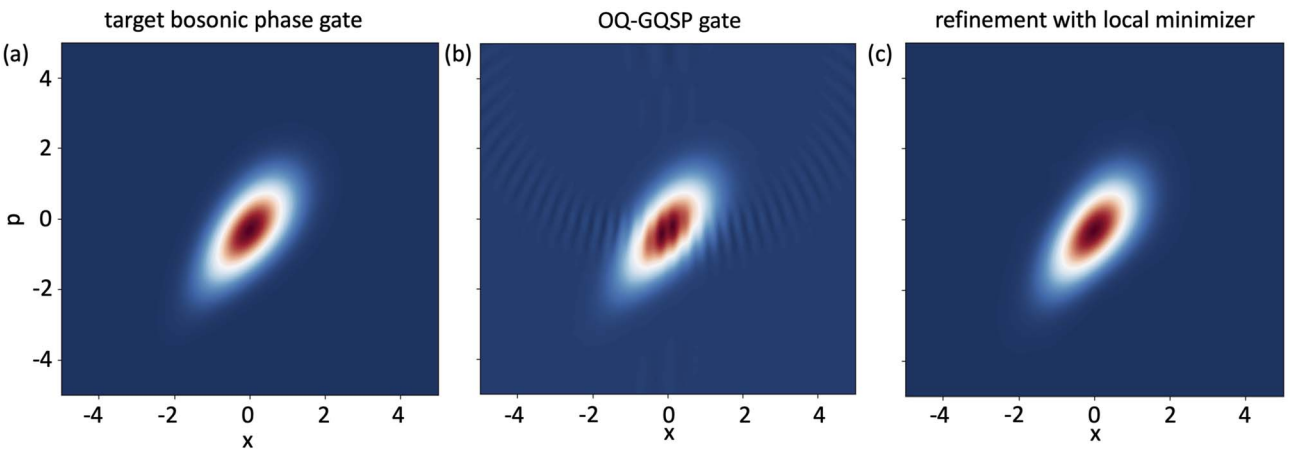

Fig. 6 Wigner function representation of the nonlinear bosonic phase gate for the ν_{26} mode Morse potential in the D_2 electronic state. (a) Target gate $e^{-iV_{26}^{(D_2)}(\hat{Q})\Delta t}$ with $\Delta t = 3.0$ fs. (b) OQ-GQSP approximation using $d = 39$ Fourier components, achieving fidelity $F = 0.9229$. (c) Numerically optimized gate using vacuum-state refinement, reaching $F = 0.9999$.

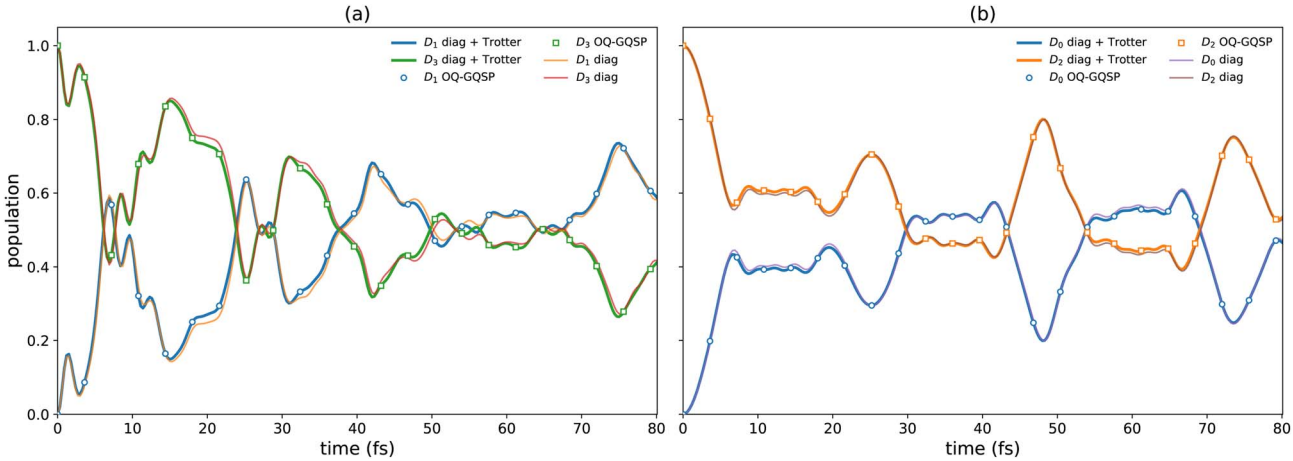

Fig. 7 Nonadiabatic population dynamics in a reduced two-mode model of the uracil cation containing the dominant harmonic mode ν_{21} and the anharmonic Morse mode ν_{26}. The total propagation time is 80.1 fs using 267 first-order Lie–Trotter steps ($\Delta t = 0.3$ fs) in a truncated oscillator Hilbert space of dimension 30 per vibrational mode. Panel (a) shows the D_3-initialized $\{D_1, D_3\}$ subspace and panel (b) shows the D_2-initialized $\{D_0, D_2\}$ subspace. Three levels of approximation are compared: "diag + Trotter" uses exact diagonalization for the nonlinear diagonal blocks within the same first-order Lie–Trotter splitting; "OQ-GQSP" replaces those diagonal blocks with the compiled OQ-GQSP phase gates under the same Trotter structure; "diag" denotes numerically exact propagation of the full projected $K = 30$ Hamiltonian without Trotterization. Each panel displays both electronic-state populations. The OQ-GQSP phase gates use 53–89 CD gates per nonlinear phase gate, with compiled phase-gate errors at the 10^{-3} level.

We observe population transfer between $|D_0\rangle$ and $|D_2\rangle$ and between $|D_1\rangle$ and $|D_3\rangle$ due to the non-zero off-diagonal elements in the vibronic coupling Hamiltonian shown in Fig. 2. Quantitatively, taking $P_{D_3}(t)$ in panel (a) and $P_{D_2}(t)$ in panel (b) as representative observables, the OQ-GQSP trajectories remain nearly indistinguishable from the "diag + Trotter" reference in both reduced subspaces: the mismatch $|P_{\mathrm{OQ}} - P_{\mathrm{diag+Trotter}}|$ peaks at only 2.94×10^{-3} in panel (a) and 1.36×10^{-4} in panel (b) over the full 80.1 fs window. By contrast, the Trotter mismatch relative to the no-Trotter "diag" propagation, $|P_{\mathrm{diag+Trotter}} - P_{\mathrm{diag}}|$, reaches 3.28×10^{-2} in panel (a) and 1.51×10^{-2} in panel (b). Thus, for this reduced model and time window, the dominant difference from the no-Trotter benchmark arises from the product formula rather than from the compiled nonlinear phase gates. Because the "diag + Trotter" and OQ-GQSP curves share the same first-order structure, their difference isolates the Fourier/QSP synthesis error in the nonlinear diagonal propagators. The Fourier truncation error ε can be systematically reduced by increasing the Fourier degree $d = \mathcal{O}(\ln \varepsilon^{-1})$; in practice we choose d from the strip-analytic bound together with direct convergence checks for the phase function and the resulting population dynamics. The SI reports an extended hierarchy including an independent MCTDH benchmark using a harmonic-oscillator discrete-variable representation (HO-DVR) primitive basis (Fig. S3). We note that the unoptimized OQ-GQSP gates provide state-independent accuracy governed by the Fourier truncation bound, while the local vacuum-state optimization offers an additional fidelity boost for near-vacuum states at no extra circuit depth cost.

5. Resource estimation

We analyze the computational resources required for OQ-GQSP and compare them with those of existing classical and quantum approaches for vibronic dynamics simulation. Our analysis addresses both asymptotic scaling and practical implementation constraints for early fault-tolerant quantum hardware. Table 1 compares the resource requirements across conventional single-layer MCTDH,[7] the digital quantum algorithm,[11,12] and our OQ-GQSP method. Each approach targets a different regime and makes trade-offs between memory, runtime, and model expressivity.

As a classical baseline, conventional single-layer MCTDH[7] exhibits exponential memory scaling with the number of particles and system coordinates and is therefore typically restricted in practice to systems with on the order of 10–15 vibrational modes, whereas multi-layer MCTDH[35] can substantially extend the accessible dimensionality for structured problems. Accordingly, our comparison is intended to emphasize the rapid growth of exact quantum-dynamical cost rather than a universal hard cutoff in the number of modes. Both quantum approaches require only polynomial quantum resources, with OQ-GQSP exploiting native bosonic modes to minimize the qubit-digitization overhead represented by $\log \mathrm{K}$ in Motlagh *et al.*[11] In the single-variate-Hamiltonian regime considered here (single-mode diagonal anharmonicity plus linear off-diagonal couplings), Motlagh's general multi-variate polynomial-term factor $\mathcal{O}(M^{d_{\mathrm{poly}}})$ reduces to $\mathcal{O}(Md_{\mathrm{poly}})$, giving the per-Trotter-step cost $\mathcal{O}(NMd_{\mathrm{poly}}^2 \log^2 K + N^2 M d_{\mathrm{poly}})$ reported in the caption of Table 1. For analytic Morse-type potentials, the polynomial-approximation degree (from Taylor, Chebyshev, or an equivalent least-squares fit) scales as $d_{\mathrm{poly}} = \mathcal{O}(\ln(1/\varepsilon))$, so Motlagh's effective accuracy scaling is $\log^2(1/\varepsilon)\log^2 K$. OQ-GQSP instead uses a single Fourier degree $d = \mathcal{O}(\ln(MN_{\mathrm{p}}/\varepsilon))$, replacing the squared polylog by a single polylog and eliminating the $\log^2 K$ qubit-digitization overhead. For genuinely multi-mode couplings (beyond the scope adopted here), the general factor

Table 1 Resource scaling comparison for vibronic dynamics simulation methods. Key differences: (1) conventional single-layer MCTDH requires exponential memory in system size but no quantum hardware; (2) Motlagh *et al.* count fault-tolerant Toffoli gates with first-order Trotterization for digital quantum computers; (3) OQ-GQSP counts CD gates with first-order Trotterization for oscillator-qubit quantum processors. The Motlagh entry is reported in its original general multi-variate form from ref. 11, consistent with the ✓ expressivity marker; for the single-variate Hamiltonian scope adopted here, the $M^{d_{\text{poly}}}$ factor reduces to $M^{d_{\text{poly}}}$, giving the per-Trotter-step cost $\mathcal{O}((NMd_{\text{poly}}{}^2\log^2 K + N^2Md_{\text{poly}})p)$; see Section V. Expressivity markers: ✓ = native coverage of the full vibronic coupling class; △ = native polylog-in-ε gate count for single-mode anharmonic potentials (diagonal directly; off-diagonal *via* the Givens-rotation reduction, SI III D); genuinely multi-mode anharmonic couplings with native polylog-in-ε gate counts might require the multivariate QSP extension of Section VI. Parameters: N = electronic states, M = vibrational modes, n_{SPF} = single-particle functions, n_{p} = MCTDH combined-mode coordinates ("particles"), d_{sys} = system coordinates, N_{basis} = primitive basis per DOF, s = Hamiltonian terms, d_{poly} = polynomial-approximation degree, K = grid points, ε = target accuracy, $p = \Gamma t^2\varepsilon^{-1}$ = Trotter layers, Γ = commutator bound, and t = simulation time

Method	Resource	Time complexity	Expressivity
Single-layer MCTDH[7]	$n_{\text{SPF}}^{n_{\text{p}}} + n_{\text{p}}n_{\text{SPF}}N_{\text{basis}}^{d_{\text{sys}}}$	$\mathcal{O}(sn_{\text{p}}^2(n_{\text{spf}})^{n_{\text{p}}+1} + sn_{\text{p}}n_{\text{spf}}N_{\text{basis}}^{2d_{\text{sys}}})$	✓
Motlagh *et al.*[11]	$\mathcal{O}((M + d_{\text{poly}}^2)\log(K) + \log(N))$ qubits	$\mathcal{O}((NM^{d_{\text{poly}}}(d_{\text{poly}}\log^2(K) + N))p)$	✓
OQ-GQSP (ours)	$N + 1$ qubits, M oscillators	$\mathcal{O}((NM\ \ln(MN_{\text{p}}/\varepsilon) + N^2M)p)$	△

$\mathcal{O}(M^{d_{\text{poly}}})$ re-emerges for both methods, and OQ-GQSP would require the multivariate QSP extension discussed in Section VI. Although OQ-GQSP achieves linear scaling with the number of vibrational modes, it is worth asking whether the success probability factor $(1-\delta)^{-2MN_{\text{p}}}$ could be a bottleneck for molecules containing numerous strongly anharmonic modes. However, the success probability decreases exponentially with the degrees of OQ-GQSP $\delta = \mathcal{O}(e^{-d})$. With only a logarithmic increase in time complexity, the success probability overhead can be made constant with respect to the system size. For the uracil cation consisting of 4 electronic states and 12 vibrational modes, there exist 5 quartic and Morse potential modes $M' = 5$. For $M'N = 20$ and target success probabilities $1 - \delta \approx 0.9988$ and 0.9997, the required number of shots increases by factors of approximately 122 and 3.14, respectively, over 100 Trotter layers. However, the corresponding OQ-GQSP degrees required to synthesize the nonlinear phase gates are 116 and 261, respectively. These values are illustrative trade-off markers under the fully coherent assumption,[26,27] although they are unlikely to be used directly in the near-term. This shows the trade-off between circuit depth and shot overhead: one may reduce the OQ-GQSP degree to shorten circuits at the expense of additional sampling overhead.

6. Discussion and conclusions

In this work, we developed a hybrid CV–DV quantum compiler that synthesizes arbitrary nonlinear bosonic phase gates with bounded error and applied it to numerical tests of simulating anharmonic vibronic dynamics of the uracil cation. The method preserves vibrational modes in their native bosonic representation while efficiently generating anharmonic potentials *via* Fourier series approximations. Numerical validation shows that OQ-GQSP captures ultrafast electronic population transfer missed by harmonic approximations. These results indicate that hybrid CV–DV processors can bridge the gap between analog LVC simulators[5,22] and fully digital vibronic dynamics simulators,[11,12] offering polynomial gate complexity in Fourier bandwidth rather than in the degree of polynomial approximation.

While OQ-GQSP represents a step toward practical molecular quantum simulation in oscillator–qubit architectures, several limitations remain. One major challenge is the exponential decay in the probability of success. A fully coherent implementation of multiplying block encoded matrices without the repeated measurements would require ancilla qubits and deeper circuits.[15] Since oscillator–qubit platforms are unlikely to operate in a fully fault-tolerant regime, and rather are likely to have advantages in near-term or early-fault tolerant devices,[6] we adopted an incoherent protocol with classical overheads instead. As shown in SI III D, single-mode off-diagonal anharmonic couplings are already compilable *via* a Givens-rotation reduction to diagonal OQ-GQSP blocks. Extending the framework to fully general multivariate nonlinear potentials $f_{nm}(\hat{Q}_0,\ldots,\hat{Q}_{M-1})$ requires multivariate QSP (M-QSP). However, efficient angle-finding techniques and complete characterization of the achievable multivariable polynomials remain open problems, despite recent progress.[36–41] From the perspective of quantum machine learning, data re-uploading—a close analogue of M-QSP—is a universal approximator for multivariate functions, although the practicality is an open problem. At least, this theory suggests that general multivariate bosonic operators can, in principle, be numerically synthesized within the M-QSP framework.[42] We have recently become aware of related simultaneous work,[43] along with an experimental demonstration on trapped ions,[44] that decomposes the Hamiltonian with a Fourier series for bosonic QSP. Specifically, their method decomposes the Hamiltonian rather than its unitary and implements each term *via* trigonometric gates, yielding analytic control parameters at the cost of an additional intra-compilation Trotter error, whereas our OQ-GQSP performs unitary-level Fourier synthesis with angles obtained numerically from the inverse nonlinear FFT on SU(2).[27] While their work focuses on generating anharmonicities and multi-mode nonlinear couplings, our OQ-GQSP framework is tailored for the constructive synthesis of state-dependent anharmonic potential propagators for multi-state electronic systems. On the hardware side, quantum error correction for oscillators remains less developed than for qubits.[45–49] More flexible non-stabilizer

bosonic codes, tailored to specific tasks, may provide a potential pathway forward. For quantum errors in the near term, recent experiments indicate passive error suppression in QSP-type sequences[50,51] and an error mitigation technique for hybrid quantum processors is suggested.[52]

We position OQ-GQSP between fully analog and fully digital approaches to molecular dynamics simulation: a compiler that preserves bosonic modes yet synthesizes anharmonic diagonal potentials with OQ-GQSP on oscillator–qubit ISAs. Recent experiments on trapped-ion and circuit QED platforms[8–10] demonstrated geometric-phase interference around CIs for minimal models, validating the concept of hybrid oscillator–qubit analog simulators.[5] Theoretical proposals for pre-Born–Oppenheimer (BO) analog simulators[22] extend this approach beyond the vibronic coupling model for harmonic potential Hamiltonians. Their coupled multi-qubit-boson mapping achieves exponential savings *versus* classical complete active space configuration interaction (CASCI)-level dynamics but still relies on Trotterized time evolution and continuous analog control of trapped-ion or circuit-QED motional modes, with resource scaling $\mathcal{O}(N_0{}^4 M^{d_{\text{poly}}})$, where N_o is the number of spin-orbitals. One may combine ref. 22 and OQ-GQSP methods leading to a generalized pre-BO framework to include anharmonic potentials in quantum simulation of coupled electron-nuclear dynamics. The fully digital quantum approach of Motlagh *et al.*[11] achieves quantum simulation for the general vibronic coupling Hamiltonian by digitizing bosonic degrees of freedom. Their singlet fission case study for a 6-state, 21-mode model requires 154 qubits and 2.76×10^6 Toffoli gates for 100 femtoseconds of dynamics, illustrating the cost of full digitization. OQ-GQSP offers a constructive middle ground: it preserves bosonic modes in their native Hilbert space while synthesizing anharmonic diagonal potentials through GQSP on oscillator–qubit ISAs. This hybrid strategy directly compiles analytic potentials into hardware-native gates, establishing a general instruction-set architecture in post-noisy-intermediate-scale-quantum (NISQ) or pre-fault-tolerant trapped-ion and circuit-QED platforms. Future work might extend the framework toward multivariate QSP for coupled anharmonic modes and explore efficient and coherent implementations without the heralded scheme.

Author contributions

Jungsoo Hong and Seong Ho Kim performed the experiments and drafted the manuscript. All authors reviewed and provided feedback on the manuscript. Seung Kyu Min and Joonsuk Huh conceived the idea, supervised the project, and reviewed the manuscript.

Conflicts of interest

There are no conflicts to declare.

Data availability

Data supporting this article have been included as part of the supplementary information (SI). Supplementary information: equations, computational details, and supplementary simulation results. See DOI: https://doi.org/10.1039/d5sc09606e.

Acknowledgements

This work was partly supported by the Basic Science Research Program through the National Research Foundation of Korea (NRF), funded by the Ministry of Science and ICT (RS-2023-NR068116, RS-2025-03532992, and RS-2024-00455131) and by the Korean ARPA-H Project *via* the Korea Health Industry Development Institute (KHIDI), funded by the Ministry of Health and Welfare, Republic of Korea (RS-2025-25456722). This work was also partly supported by the Institute for Information & communications Technology Promotion (IITP) grant funded by the Korean government (MSIP) (No. 2019-0-00003, Research and Development of Core technologies for Programming, Running, Implementing and Validating of Fault-Tolerant Quantum Computing Systems). JH is supported by the Yonsei University Research Fund of 2025-22-0140.

References

1 Y. Liu, S. Singh, K. C. Smith, E. Crane, J. M. Martyn, A. Eickbusch, A. Schuckert, R. D. Li, J. Sinanan-Singh, M. B. Soley, T. Tsunoda, I. L. Chuang, N. Wiebe and S. M. Girvin, Hybrid oscillator-qubit quantum processors: Instruction set architectures, abstract machine models, and applications, 2025, *arXiv*, preprint, arXiv:2407.10381, DOI: 10.48550/arXiv.2407.10381.

2 O. Hahn, G. Ferrini and R. Takagi, Bridging magic and non-gaussian resources via gottesman-kitaev-preskill encoding, *PRX Quantum*, 2025, **6**, 010330.

3 A. Sørensen and K. Mølmer, Entanglement and quantum computation with ions in thermal motion, *Phys. Rev. A*, 2000, **62**, 022311.

4 A. Eickbusch, V. Sivak, A. Z. Ding, S. S. Elder, S. R. Jha, J. Venkatraman, B. Royer, S. M. Girvin, R. J. Schoelkopf and M. H. Devoret, Fast universal control of an oscillator with weak dispersive coupling to a qubit, *Nat. Phys.*, 2022, **18**, 1464.

5 R. J. MacDonell, C. E. Dickerson, C. J. T. Birch, A. Kumar, C. L. Edmunds, M. J. Biercuk, C. Hempel and I. Kassal, Analog quantum simulation of chemical dynamics, *Chem. Sci.*, 2021, **12**, 9794.

6 M. Kang, H. Nuomin, S. N. Chowdhury, J. L. Yuly, K. Sun, J. Whitlow, J. Valdiviezo, Z. Zhang, P. Zhang, D. N. Beratan and K. R. Brown, Seeking a quantum advantage with trapped-ion quantum simulations of condensed-phase chemical dynamics, *Nat. Rev. Chem.*, 2024, **8**, 340.

7 G. A. Worth, H.-D. Meyer, H. Köppel, L. S. Cederbaum and I. Burghardt, Using the MCTDH wavepacket propagation method to describe multimode non-adiabatic dynamics, *Int. Rev. Phys. Chem.*, 2008, **27**(3), 569–606.

8 C. Valahu, V. Olaya-Agudelo, R. MacDonell, T. Navickas, A. Rao, M. Millican, J. Pérez-Sánchez, J. Yuen-Zhou, M. Biercuk, C. Hempel, T. Tan and I. Kassal, Direct observation of geometric-phase interference in dynamics around a conical intersection, *Nat. Chem.*, 2023, **15**, 1503.
9 J. Whitlow, Z. Jia, Y. Wang, C. Fang, J. Kim and K. Brown, Quantum simulation of conical intersections using trapped ions, *Nat. Chem.*, 2023, **15**, 1509.
10 C. S. Wang, N. E. Frattini, B. J. Chapman, S. Puri, S. M. Girvin, M. H. Devoret and R. J. Schoelkopf, Observation of wave-packet branching through an engineered conical intersection, *Phys. Rev. X*, 2023, **13**, 011008.
11 D. Motlagh, R. A. Lang, P. Jain, J. A. Campos-Gonzalez-Angulo, W. Maxwell, T. Zeng, A. Aspuru-Guzik and J. Miguel Arrazola, Quantum algorithm for vibronic dynamics: case study on singlet fission solar cell design, *Quantum Sci. Technol.*, 2025, **10**, 045048.
12 S. Malpathak, S. D. Kallullathil and A. F. Izmaylov, Simulating vibrational dynamics on bosonic quantum devices, *J. Phys. Chem. Lett.*, 2025, **16**, 1855, DOI: 10.1021/acs.jpclett.4c03480.
13 D. Motlagh and N. Wiebe, Generalized quantum signal processing, *PRX Quantum*, 2024, **5**, 020368.
14 S. Matsika, Two- and three-state conical intersections in the uracil cation, *Chem. Phys.*, 2008, **349**, 356.
15 F. Vasconcelos and A. Gilyén, Methods for reducing ancilla-overhead in block encodings, 2025, *arXiv*, preprint, arXiv:2507.07900, DOI: 10.48550/arXiv.2507.07900.
16 J. Y. Araz, M. Grau, J. Montgomery and F. Ringer, Hybrid quantum simulations with qubits and qumodes on trapped-ion platforms, *Phys. Rev. A*, 2025, **112**, 012620.
17 M. Assmann, H. Köppel and S. Matsika, Photoelectron spectrum and dynamics of the uracil cation, *J. Phys. Chem. A*, 2015, **119**, 866.
18 S. Matsika, M. Spanner, M. Kotur and T. C. Weinacht, Ultrafast relaxation dynamics of uracil probed via strong field dissociative ionization, *J. Phys. Chem.*, 2013, **117**, 12796.
19 M. Kotur, C. Zhou, S. Matsika, S. Patchkovskii, M. Spanner and T. C. Weinacht, Neutral-ionic state correlations in strong-field molecular ionization, *Phys. Rev. Lett.*, 2012, **109**, 203007.
20 J. Segarra-Martí, T. Tran and M. J. Bearpark, Ultrafast and radiationless electronic excited state decay of uracil and thymine cations: computing the effects of dynamic electron correlation, *Phys. Chem. Chem. Phys.*, 2019, **21**, 14322.
21 P. Vindel-Zandbergen, S. Matsika and N. T. Maitra, Exact-factorization-based surface hopping for multistate dynamics, *J. Phys. Chem. Lett.*, 2022, **13**, 1785.
22 J.-K. Ha and R. J. MacDonell, Analog quantum simulation of coupled electron-nuclear dynamics in molecules, *Chem. Sci.*, 2025, **16**(41), 19423–19435.
23 O. Katz, M. Cetina and C. Monroe, Programmable *n*-body interactions with trapped ions, *PRX Quantum*, 2023, **4**, 030311.
24 G. H. Low, T. J. Yoder and I. L. Chuang, Methodology of resonant equiangular composite quantum gates, *Phys. Rev. X*, 2016, **6**, 041067.
25 K. Park and R. Filip, Efficient bosonic nonlinear phase gates, *npj Quantum Inf.*, 2024, **10**, 25.
26 L. Laneve, Generalized quantum signal processing and non-linear fourier transform are equivalent, 2025, *arXiv*, preprint, arXiv:2503.03026, DOI: 10.48550/arXiv.2503.03026.
27 H. Ni, R. Sarkar, L. Ying and L. Lin, Inverse nonlinear fast fourier transform on su(2) with applications to quantum signal processing, 2025, *arXiv*, preprint, arXiv:2505.12615, DOI: 10.48550/arXiv.2505.12615.
28 Y. Liu, J. M. Martyn, J. Sinanan-Singh, K. C. Smith, S. M. Girvin, and I. L. Chuang, Toward mixed analog-digital quantum signal processing: Quantum ad/da conversion and the fourier transform, 2025, *arXiv*, preprint, arXiv:2408.14729, DOI: 10.48550/arXiv.2408.14729.
29 J. M. Martyn, Y. Liu, Z. E. Chin and I. L. Chuang, Efficient fully-coherent quantum signal processing algorithms for real-time dynamics simulation, *J. Chem. Phys.*, 2023, **158**, 024106.
30 S. Yamamoto and N. Yoshioka, Robust angle finding for generalized quantum signal processing, 2024, *arXiv*, preprint, arXiv:2402.03016, DOI: 10.48550/arXiv.2402.03016.
31 D. Leibfried, R. Blatt, C. Monroe and D. Wineland, Quantum dynamics of single trapped ions, *Rev. Mod. Phys.*, 2003, **75**, 281.
32 S. Krastanov, V. V. Albert, C. Shen, C.-L. Zou, R. W. Heeres, B. Vlastakis, R. J. Schoelkopf and L. Jiang, Universal control of an oscillator with dispersive coupling to a qubit, *Phys. Rev. A*, 2015, **92**, 040303.
33 A. M. Childs, Y. Su, M. C. Tran, N. Wiebe and S. Zhu, Theory of trotter error with commutator scaling, *Phys. Rev. X*, 2021, **11**, 011020.
34 W.-C. Lin and C.-H. Wang, Analog quantum phase estimation with single-mode readout, 2025, *arXiv*, preprint, arXiv:2506.15668, DOI: 10.48550/arXiv.2506.15668.
35 H. Wang, Multilayer multiconfiguration time-dependent hartree theory, *J. Phys. Chem.*, 2015, **119**, 7951, DOI: 10.1021/acs.jpca.5b03256.
36 Z. M. Rossi and I. L. Chuang, Multivariable quantum signal processing (M-QSP): prophecies of the two-headed oracle, *Quantum*, 2022, **6**, 811.
37 H. Mori, K. Mizuta and K. Fujii, Comment on "Multivariable quantum signal processing (M-QSP): prophecies of the two-headed oracle, *Quantum*, 2024, **8**, 1512.
38 B. Németh, B. Kövér, B. Kulcsár, R. B. Miklósi and A. Gilyén, On variants of multivariate quantum signal processing and their characterizations, 2023, *arXiv*, preprint, arXiv:2312.09072, DOI: 10.48550/arXiv.2312.09072.
39 Y. Ito, H. Mori, K. Sakamoto and K. Fujii, Polynomial time constructive decision algorithm for multivariable quantum signal processing, 2025, *arXiv*, preprint, arXiv:2410.02332, DOI: 10.48550/arXiv.2410.02332.
40 L. Laneve and S. Wolf, On multivariate polynomials achievable with quantum signal processing, *Quantum*, 2025, **9**, 1641.

41 L. Laneve, An adversary bound for quantum signal processing, 2025, *arXiv*, preprint, arXiv:2506.20484, DOI: 10.48550/arXiv.2506.20484.
42 A. Pérez-Salinas, M. Y. Rad, A. Barthe and V. Dunjko, Universal approximation of continuous functions with minimal quantum circuits, 2025, *arXiv*, preprint, arXiv:2411.19152, DOI: 10.48550/arXiv.2411.19152.
43 T. Chalermpusitarak, K. Schwennicke, I. Kassal and T. R. Tan, Programmable generation of arbitrary continuous-variable anharmonicities and nonlinear couplings, 2025, *arXiv*, preprint, arXiv:2511.22286, DOI: 10.48550/arXiv.2511.22286.
44 C. McGarry, T. Chalermpusitarak, K. Schwennicke, F. Scuccimarra, M. J. Millican, V. G. Matsos, C. H. Valahu, P. Nagpal, H.-K. Chan, *et al.*, Programmable quantum simulation of anharmonic dynamics, 2026, *arXiv*, preprint, arXiv:2603.04744, DOI: 10.48550/arXiv.2603.04744.
45 J. Niset, J. Fiurášek and N. J. Cerf, No-go theorem for gaussian quantum error correction, *Phys. Rev. Lett.*, 2009, **102**, 120501.
46 C. Vuillot, H. Asasi, Y. Wang, L. P. Pryadko and B. M. Terhal, Quantum error correction with the toric gottesman-kitaev-preskill code, *Phys. Rev. A*, 2019, **99**, 032344.
47 K. Noh, S. M. Girvin and L. Jiang, Encoding an oscillator into many oscillators, *Phys. Rev. Lett.*, 2020, **125**, 080503.
48 J. Wu and Q. Zhuang, Continuous-variable error correction for general gaussian noises, *Phys. Rev. Appl.*, 2021, **15**, 034073.
49 J. Wu, A. J. Brady and Q. Zhuang, Optimal encoding of oscillators into more oscillators, *Quantum*, 2023, **7**, 1082.
50 J.-T. Bu, L. Zhang, Z. Yu, J.-B. Wang, W.-Q. Ding, W.-F. Yuan, B. Wang, H.-J. Du, W.-J. Chen, L. Chen, J.-W. Zhang, J.-C. Li, F. Zhou, X. Wang and M. Feng, Exploring the experimental limit of deep quantum signal processing using a trapped-ion simulator, *Phys. Rev. Appl.*, 2025, **23**, 034073.
51 S. Zeytinoğlu and S. Sugiura, Error-robust quantum signal processing using rydberg atoms, *Phys. Rev. Res.*, 2024, **6**, 013003.
52 K. Park, J. Hastrup, J. S. Neergaard-Nielsen, J. B. Brask, R. Filip and U. L. Andersen, Slowing quantum decoherence of oscillators by hybrid processing, *npj Quantum Inf.*, 2022, **8**, 67.